

Article

Experimentally Validated Modelling of an Oscillating Diaphragm Compressor for Chemisorption Energy Technology Applications

Ahmad Najjaran, Saleh Meibodi, Zhiwei Ma *, Huashan Bao and Tony Roskilly

Department of Engineering, Durham University, Durham DH1 3LE, UK

* Correspondence: zhiwei.ma@durham.ac.uk

Abstract: This study presents a detailed dynamic modelling and generic simulation method of an oscillating diaphragm compressor for chemisorption energy technology applications. The geometric models of the compressor were developed step by step, including the diaphragm movement, compressor dimensions, chamber areas and volumes and so on. The detailed mathematical model representing the geometry and kinematics of the diaphragm compressor was combined with the motion equation, heat transfer equation and energy balance equation to complete the compressor modelling. This combination enables the novel compressor model to simultaneously handle the simulation of momentum and energy balance of the diaphragm compressor. Furthermore, an experimental apparatus was set up to investigate and validate the present modelling and the simulation method. The performance of the compressor was experimentally evaluated in terms of the mass flow rate of the compressor at various compression ratios. Additionally, the effects of different parameters such as the inlet temperature and ambient temperature at various compressor ratios on the compressor performance were investigated. It was found reducing the inlet temperature from 40 to 5 °C at a constant pressure results in the enhancement of the compressor flow rate up to 14.7%. The compressor model proposed and developed in this study is shown to be not only able to accurately deal with the complexity of the dynamic behaviour of the compressor working flow but is also capable of effectively representing diaphragm compressors for analysis and optimisation purposes in various applications.



Citation: Najjaran, A.; Meibodi, S.; Ma, Z.; Bao, H.; Roskilly, T. Experimentally Validated Modelling of an Oscillating Diaphragm Compressor for Chemisorption Energy Technology Applications. *Energies* **2023**, *16*, 489. <https://doi.org/10.3390/en16010489>

Academic Editor: Rafael J. Bergillos

Received: 12 November 2022

Revised: 23 December 2022

Accepted: 28 December 2022

Published: 2 January 2023



Copyright: © 2023 by the authors. Licensee MDPI, Basel, Switzerland. This article is an open access article distributed under the terms and conditions of the Creative Commons Attribution (CC BY) license (<https://creativecommons.org/licenses/by/4.0/>).

Keywords: oscillating diaphragm compressor; modelling and simulation; experimental validation; compressor performance

1. Introduction

In order to enhance energy efficiency and cost-effectiveness, many research efforts have been conducted to maximise the use of renewable energy sources, such as solar, wind, and geothermal. Several thermodynamic cycles have been proposed and studied to generate energy from low-grade heat. These include the organic Rankine cycle, sorption cycles, and chemisorption cycles as a stand-alone energy system or in a district heating context [1–5]. In order to improve the efficiency of power cycles, scientists removed mechanical components from the power cycle in order to examine their performance without moving parts and modify the geometrical configurations of other components to improve the cycle performance. Von Platen introduced an innovation in the 1920s based on removing pumps from the absorption cycle [6]. Since then, other geometrical adoptions have been performed to maximise or optimise the performance of the cycle. However, all the attempts ended up with a cycle coefficient of performance (COP) no better than 0.3 [7–10].

Improvement and enhancement of energy performance of energy systems have always been the main objectives of research activities. In an earlier study, Von Platen introduced an innovative absorption cycle operating without pumps and showed cycle performance improvement [6]. Since then, other geometrical adoptions have been performed to maximise

or optimise the performance of the cycle. However, all the attempts ended up with cycle COP no better than 0.3 [7–10]. There is also the possibility to introduce innovations in the power cycle by incorporating assisting mechanical or electrical components. For instance, it has been demonstrated that adding an electric heater or a compressor to a thermochemical sorption cycle can improve heating, cooling and power generation [11,12].

Adding a compressor to the thermochemical sorption cycle is a promising modification for energy storage, or more specifically for solar seasonal energy storage, particularly in regions where solar irradiance is available at least partially all year round [11,13,14]. However, it is challenging and sophisticated to mathematically model the thermodynamic compressor process, mainly due to the highly dynamic behaviour of the working fluids in a compressor. Compressor type and efficiency, along with the working fluid and ambient conditions (for example, temperature and humidity), are all critical parameters to consider once a compressor is used in thermodynamic processes as an assisting component. Hence, it is necessary to model compressors individually in order to understand their dynamic behaviours as they interact with other components and have a noticeable impact on the overall COP of systems.

Therefore, improving compressor performance is crucial as it saves energy and produces more work with the same amount of time [15–17]. The compressor's performance has been studied for various applications in different sectors such as power systems [18,19], heat pumps, waste heat recovery [20], and even in fuel cell industry [21]. Energy consumption reduction in thermodynamic cycles can be one of the motivations for developing compressors' performance; for instance, by developing high-efficiency compressors, wastewater aeration can be made to save 2.5% to 4.9% of the energy used annually in wastewater treatment processes [22]. Increasing the efficiency of a compressor can be achieved by understanding the effect of various compressor parameters on performance [23]. Using a compressor model is helpful for researchers who wish to study the performance of a compressor with operating inputs. Compressors are commonly seen as simple mechanical structures with simple motions that can be described mathematically by using thermodynamic equations that describe the motion.

An example is the study of a mathematical model for a reciprocating compressor in order to predict the thermodynamic behaviour and valve motion under different crank angles [24]. As a part of another study, an analytical approach involving a diaphragm compressor controlled by an electrostatic actuator mechanism (EAM) was used to model a miniature-scale refrigeration system using an EAM. In the model, it is assumed that the circular flexible diaphragm is mounted on a circular clamp and surrounded by a conformal chamber that surrounds the diaphragm. It is determined that the maximum voltage required to compress the refrigerant R134a gas to 30 kPa, is approximately 400 volts. It is anticipated that the pressure rise is less than required to perform an electronic cooling application when the system is implemented in a series of diaphragm compressors united in an array [25].

There are some researchers that considered modelling the turbomachines such as pumps to develop a model by considering its geometrical design [26]; however, for a diaphragm compressor, a further study needs to be carried on. An ideal model assuming isobaric suction and discharge processes are introduced in some studies. However, the standard model can only be applied to some simplified cases. In most compressor studies, other solutions are necessary to deal with the nonlinear variations of the problem. Moreover, a simplified model is assumed to ignore factors that might significantly affect compressor performance. Therefore, an accurate model considering more is required for optimisation.

This study aims to develop and validate a detailed model of a diaphragm compressor. Detailed geometric dimensions were used to describe the volume change. Heat transfer and valve motion were discussed. To predict the instantaneous heat transfer in reciprocating compressors through the wall of the compression chamber, various correlations have been reported in present investigations [27]. An appropriate correction for this model is selected. Complex valve motion was treated as a beam deflection problem contributing

to a reasonable flow rate. Instead of assuming a smooth valve motion, valve oscillation based on the pressure conditions was designed. Together with thermodynamic balance equations, the simulation was implemented in MATLAB. This paper does not consider the ideal gas assumption for the working fluid (air); therefore, air humidity and other thermodynamic properties are calculated. To this end, this paper provides figures on pressure and temperature performance. The simulated flow rate was validated against experimental results, and the comparison showed reasonable correction. The influence of valve dimensions on flow rate was discussed graphically.

2. Diaphragm Compressor Working Principals

A diaphragm compressor (Figure 1) can be identified as a variant of the reciprocating compressor with backup and piston rings and rod seal. Rather than the intake element in reciprocating compressors, the compression process occurs by utilising a diaphragm (flexible membrane) [28]. Due to the movement of the diaphragm driven by a crankshaft mechanism, the pump gas is compressed while it is only in contact with the diaphragm and the compressor box. This feature enables this type of compressor to suitably compress a wide range of gasses, including explosive, corrosive and toxic gases.

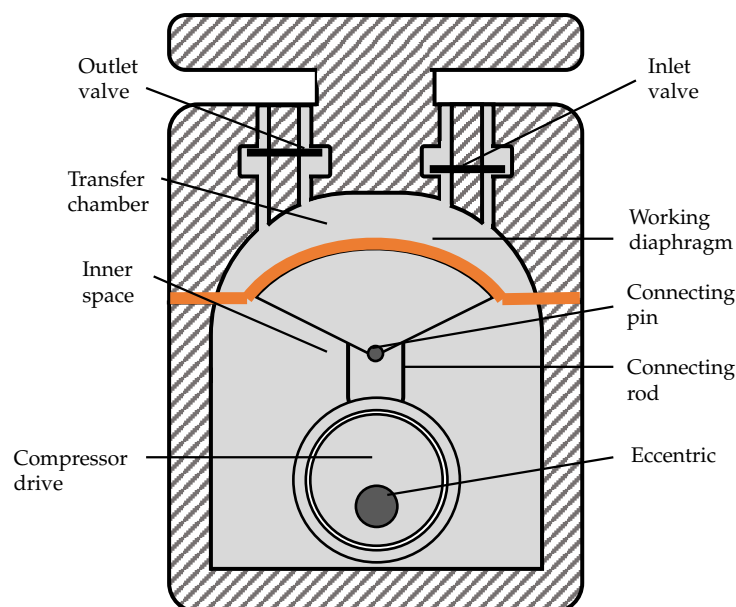
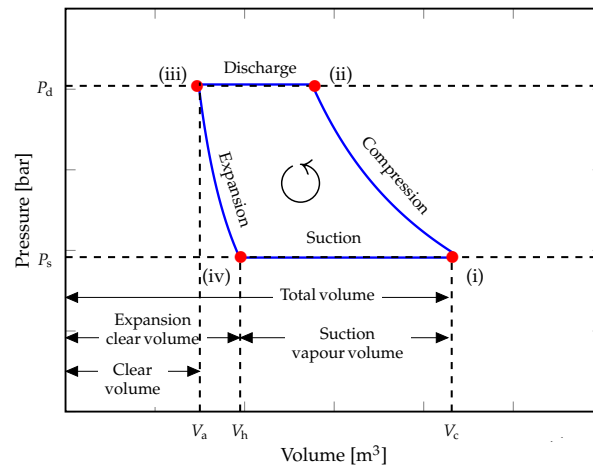


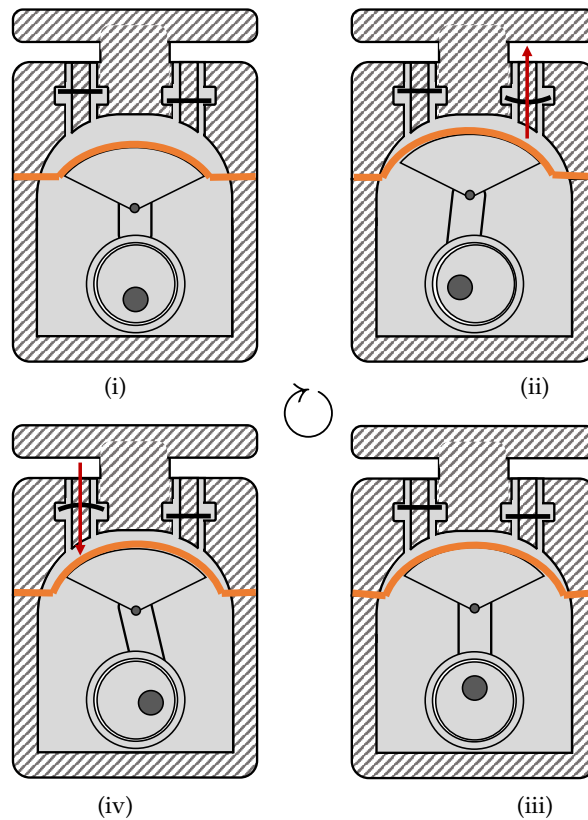
Figure 1. The section view of a diaphragm compressor cylinder/compression compartment, with the details of the internal component.

The compressing process and the corresponding Pressure-Volume relationship and variation of the compression process are illustrated in Figure 2a. In the figure, (i)–(ii) process is the compression process, (ii)–(iii) is the discharge process, (iii)–(iv) is the expansion process and (iv)–(i) is the suction process. Theoretically, the suction and discharge processes can be an isobaric process considering perfect valves (no pressure drop and no leakage or with fixed pressure drop); the polynomial compression/expansion process depends on internal leakage and heat loss. The corresponding visual illustration of each step of compressing cycle using a diaphragm compressor and the position of the diaphragm in each stage are illustrated in Figure 2b. According to Figure 3, the process consists of two isobaric stages and two stages in which pressure and volume are changed. The compressor at State (i) has the maximum gas volume as the crankshaft is at the lowest position. As the shaft clockwise rotates, the connecting rod and piston/diaphragm move up. Therefore, the gas volume decreases along with the pressure increase. Once the pressure inside the compressor is higher than the back pressure, the outlet reed valve is forced to open and allow the gas discharge until the diaphragm is pushed to the top and the gas volume

reaches the minimum value in State (ii). As the shaft continuously rotates, the diaphragm moves backwards, the chamber volume increases and the gas inside the compressor is then expanded in State (iii). Once the pressure inside the compressor is lower than the inlet gas pressure, the inlet reed valve is forced to open and allow the gas to enter until the diaphragm is pulled to the bottom position in State (iv). When the gas volume reaches the maximum value, it returns to its initial state.



(a)



(b)

Figure 2. Principle of the compressor. (a) P-V diagram of the compression process of the compressor, (b) the geometrical schematic of the compression compartment and the diaphragm position in corresponding stages in Figure 2a and the reed valve status in each stage (i to ii is the compression, ii to iii is the discharge, iii to iv is the expansion and iv to i is the suction stage).

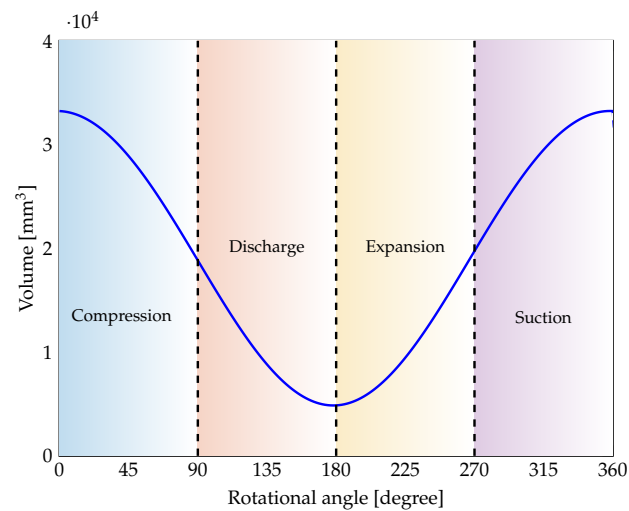


Figure 3. The volume change based on the rotational angle of the compressor for each compression, discharge, expansion and suction.

3. Model Development

The modelling and simulation of the diaphragm compressor were deemed sophisticated due to the complicated geometry and movement. Therefore, diaphragm compressor modelling cannot be accurate without considering all the details associated with the geometry and the thermodynamic process of the compression. The following details of the compressor geometry, the mathematical model for diaphragm movement, and the gas volume variation of the compressor during the operation will be described. Furthermore, the thermodynamic methodology developed to solve the thermodynamic states of the working fluid at each point of the compressor rotation will be explained. It is followed by assessing diaphragm compressor efficiency under various working conditions. The modelling results will be compared against two set of results. The first one is the experimental data obtained from a set of experiments designed and conducted in this research and the other one is the performance profile provided by the compressor manufacturer.

3.1. Geometry Description of Diaphragm Compressor

The diaphragm compressor used in this research for modelling and experimental investigation is a double diaphragm compressor supplied by KNF (the model No.: N186.1.2 ST.13 E), the photo of which is shown in Figure 4. The working gas in the current study is air; however, other gases, e.g., ammonia, can be chosen as a working fluid without requiring any modification. The compressor uses a working PTFE-coated diaphragm and an additional safety diaphragm preventing the gas from escaping in the event of a fracture. The maximum operating pressure is 6 bar (absolute value). The compressor has a high level of gas tightness; it can also be used as a vacuum pump to an ultimate vacuum of 0.13 bar (absolute value). The flow rate at the atmospheric pressure and ambient temperature is 35 L/min. The permissible ambient and media temperatures are both 5 °C and 40 °C, respectively.

Based on the section view of the compressor in Figure 1 the compartment consist of two reed valve which are responsible for charging and discharging the gas in the compartment. Once the working gas moves in the compartment, it is trapped between the diaphragm and the top head of the compartment in the transfer chamber and there is no gas at the bottom of the diaphragm. There is an eccentric shaft configuration at the bottom of the crank to guarantee the cyclic rotational movement of the diaphragm.

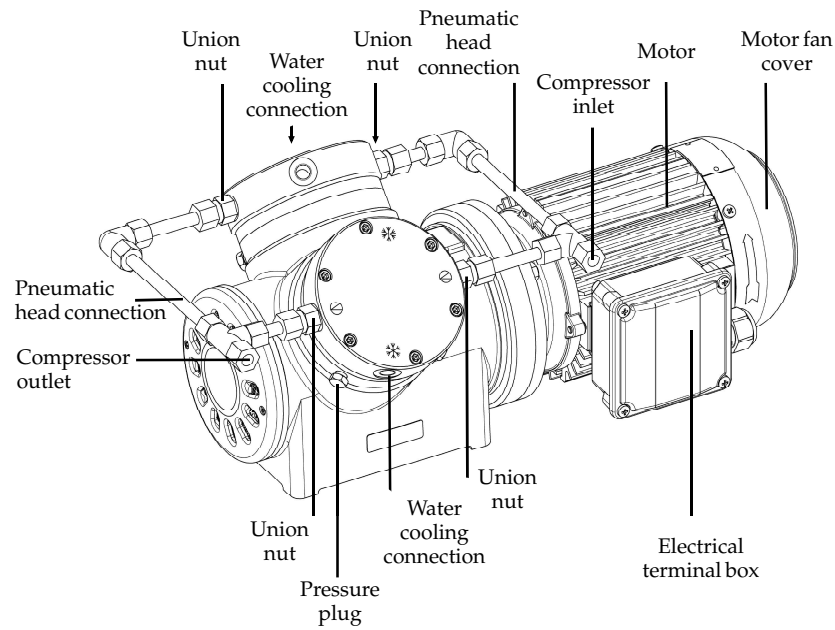


Figure 4. A 3-D representation of a schematic diagram of a KNF compressor and its component.

According to Figure 5 the essential parameters for the calculation of the gas volume of the compressor are the radius of the cylinder top curve R_1 , its height δ_1 and width D_1 , the radius of piston top curve R_2 , its height δ_2 and width D_2 , the radius of the eccentric shaft rotation circle R_3 , and the height of the diaphragm H_1 . The values of these essential parameters are derived from the manufacturer data and are presented in Table 1. In the following, the mathematical model for calculating the gas volume variation of the compressor is presented.

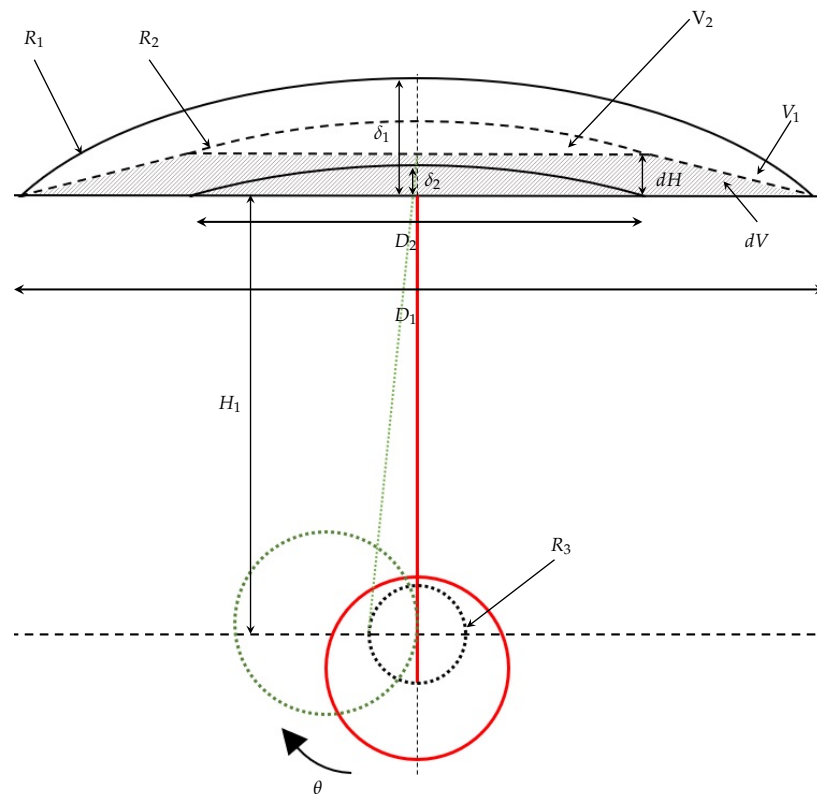


Figure 5. The geometrical properties of the elements which are effective in the current model.

Table 1. The geometrical parameter values of the compressor.

Parameters	R_1	δ_1	D_1	R_2	δ_2	D_2	R_3	D_3
Unit	[mm]	[mm]	[mm]	[mm]	[mm]	[mm]	[mm]	[mm]
Value	116	10.17	95	90	3.47	49.5	3.35	97.16

The rotation of the crankshaft results in the movement of the elastic diaphragm leading to the volume variation of the transfer chamber. Thus, The gas volume variation can be described concerning the height of the working diaphragm. Given the rotational angle, θ , the highest distance between the eccentric and diaphragm L_0 , the lift of the diaphragm, dH , can be described based on the dimensions shown in Figure 5, as below:

$$L_0 = \sqrt{(H_1 + \delta_2 + R_3)^2 - R_3^2 \sin^2 \theta} \tag{1}$$

$$dH = L_0 - H_1 - \delta_2 - R_3 \cos \theta \tag{2}$$

where δ_2 is the distance between the sphere cap of the connecting rod and the initial position, and δ_1 refers to the distance between the top of the transfer chamber and the initial position. These two parameters can be calculated as follows:

$$\delta_2 = R_2 - \sqrt{R_2^2 - \frac{D_2^2}{2}} \tag{3}$$

$$\delta_1 = R_1 - \sqrt{R_1^2 - \frac{D_1^2}{2}} \tag{4}$$

where R_1 is the radius of the upper wall of the chamber, and R_2 is the radius of the sphere cap. D_1 and D_2 are the diameters of the bottom plate and the top plate of the truncated cone, respectively. Initially, the diaphragm lifts dH_0 equal to zero, i.e., eccentric rotates to the lowest. With the rotation of the shaft, the variation of the height of the diaphragm varies to the maximum, equal to:

$$dH = L_0 - H_1 - \delta_2 + R_3, \tag{5}$$

The volume of working gas inside the transfer chamber (V) can be calculated as

$$V_c = V_1 - V_2 - dV, \tag{6}$$

where V_1 is the total volume including the volume of sphere cap, V_2 is the volume of the truncated cone, and dV is the variation of gas volume that can be expressed in terms of the rotation angle. The volumes can be defined as:

$$\begin{aligned} V_1 &= \pi \delta_1^2 \left(R_1 - \frac{\delta_1}{3} \right) \\ V_2 &= \pi \delta_2^2 \left(R_2 - \frac{\delta_2}{3} \right) \\ dV &= \frac{1}{3} \pi dH \frac{D_1^2 + D_2^2 + D_1 D_2}{4} \end{aligned} \tag{7}$$

Therefore, the compressor volume can be calculated as a function of the rotation angle (θ), by replacing L_0, dh from Equations (1) and (2), respectively, into Equation (6), as follows:

$$\begin{aligned} V_c &= \pi \delta_1^2 \left(R_1 - \frac{\delta_1}{3} \right) - \pi \delta_2^2 \left(R_2 - \frac{\delta_2}{3} \right) - \frac{1}{3} \left(\sqrt{(H_1 + \delta_2 + R_3)^2 - R_3^2 \sin^2 \theta} \right. \\ &\quad \left. - H_1 - \delta_2 - R_3 \cos \theta \right) \left(\frac{D_1^2 + D_2^2 + D_1 D_2}{4} \right) \end{aligned} \tag{8}$$

The gas volume variation in the function of the rotational angle is shown in Figure 2b, each cycle is split into 4 quarters. It is assumed that the cycle is started by compression, discharge, expansion, and suction. The minimum volume is not zero (4856 mm^3) due to the existence of the dead volume in the cylinder compartment.

3.2. Thermodynamics Modelling

The compressor cycle follows the first law of thermodynamic in an open control volume, and can be defined as:

$$\frac{d(mu)}{dt} = \dot{Q} - P \frac{dV}{dt} + \dot{m}_{in}h_{in} - \dot{m}_{out}h_c \quad (9)$$

where m is the mass of the gas inside the control volume (the mass trapped in the space between the diaphragm and the cylinder head), u is the internal energy, \dot{Q} is the heat transferred from the surroundings to the gas, P is the pressure, V is the volume, t is the time, \dot{m}_{in} is the inlet gas mass flow rate, h_{in} is the inlet gas enthalpy, \dot{m}_{out} is the outlet gas mass flow rate, h_{out} is the gas enthalpy. The equation can be reorganised by replacing internal energy u with $h-Pv$ (v is the specific volume) as given in following equations:

$$\frac{d(mh - PV)}{dt} = \dot{Q} - P \frac{dV}{dt} + \dot{m}_{in}h_{in} - \dot{m}_{out}h_{out} \quad (10)$$

$$\frac{d(mh)}{dt} = \dot{Q} + V \frac{dP}{dt} + \dot{m}_{in}h_{in} - \dot{m}_{out}h_{out} \quad (11)$$

$$m \frac{dh}{dt} + h \frac{dm}{dt} = \dot{Q} + V \frac{dP}{dt} + \dot{m}_{in}h_{in} - \dot{m}_{out}h_{out} \quad (12)$$

Therefore, for compression stage ((i)–(ii)) and expansion ((iii)–(iv)) processes in Figure 2a, by considering no gas entering and exiting, Equation (6) yields to:

$$m \frac{dh}{dt} = \dot{Q} + V \frac{dP}{dt} \quad (13)$$

On the other hand, while there is no gas exiting the compression compartment in the suction stage, Equation (12) yields to:

$$m \frac{dh}{dt} + h \frac{dm}{dt} = \dot{Q} + V \frac{dP}{dt} + \dot{m}_{in}h_{in} \quad (14)$$

For gas discharge process ((iv)–(i)) process, no gas entering is considered; therefore, Equation (12) turns into:

$$m \frac{dh}{dt} = \dot{Q} + V \frac{dP}{dt} \quad (15)$$

The heat transfer between the gas inside the compressor and the ambient air (\dot{Q}) can be determined based on the empirical equations proposed by Tuhovcak et al. [29]:

$$Nu = a Re^b Pr^c \quad (16)$$

where Nu is the Nusselt number, Re is the Reynolds number, Pr is the Prandtl number, a , b and c are constants defined by Tuhovcak et al. [29]. Due to the movement of the piston, Reynolds number and constants are different for suction, compression, discharge and expansion processes, which are detailed in Table 2. The V_p is the piston speed, V_c is the effective gas velocity caused by suction or discharge which can be calculated by the following equation:

$$V_c = |\dot{m}| |A_c| \rho \quad (17)$$

where \dot{m} is the mass flow rate of gas, A_c is the cross sectional area of the cylinder, ρ is the density of gas inside the cylinder. By knowing the Re , Pr , V_c , and other parameters, one can find the heat transfer coefficient (h_c) from:

$$h_c = \frac{Nu k}{l} \quad (18)$$

where k is the thermal conductivity of the compressor wall, and l is the characteristic length of the compressor chamber which is the ratio of the volume to the area. then, it yields to:

$$\dot{Q} = h A (T_{amb} - T) \quad (19)$$

where \dot{Q} is the heat transfer, h is the heat transfer coefficient, A is the area and T is the temperature of the gas.

Table 2. The heat transfer parameter values of a diaphragm compressor [29].

Process	Reynolds Number	a	b	c
Compression	$\rho D V_p / \mu$	0.08	0.8	0.6
Discharge	$(\rho D V_p + V_p^{0.8} V_c^{0.2}) / \mu$	0.08	0.8	0.6
Expansion	$\rho D V_p / \mu$	0.12	0.8	0.6
Suction	$(\rho D V_p + V_p^{-0.4} V_c^{1.4}) / \mu$	0.08	0.9	0.6

3.3. Modelling Algorithm

The following assumptions have been made to reasonably simplify the simulation of the compressor performance.

- The gas leakage through the reed valve is negligible;
- The rotation speed of the compressor is initially pre-defined at a fixed value;
- The pressure drop through the reed valve is pre-defined at a fixed value, therefore the gas pressure has no change during suction and discharge stages;
- Gas is uniformly distributed inside the compressor;

Air was used as working gas for this simulation and validation. Thermo-physical properties of air, including specific heat, density, enthalpy, thermal conductivity and viscosity, were correlated as the function of temperature, pressure and humidity [30,31]. The simulation process is detailed as follows:

- The pre-defined rotational speed is used to determine the time interval and rotational angel at present calculation step;
- The present rotational angel is used to determine the present volume;
- The present rotational angel and previous gas pressure are used to determine which stage of the process among compression, discharge, expansion and suction;
- The thermodynamic equation and heat transfer equation are called to calculate the present gas pressure, temperature and other properties;
- The mass flow rates in suction and discharge stages are determined based on the assumed constant gas pressure caused by the assumption of fixed pressure drop through reed valves.
- The time step is 0.0005 s to make sure that all the short-timescale dynamic effects are captured in the model, and the process is modelled for 20 s.

The flowchart diagram of the model is illustrated in Figure 6.

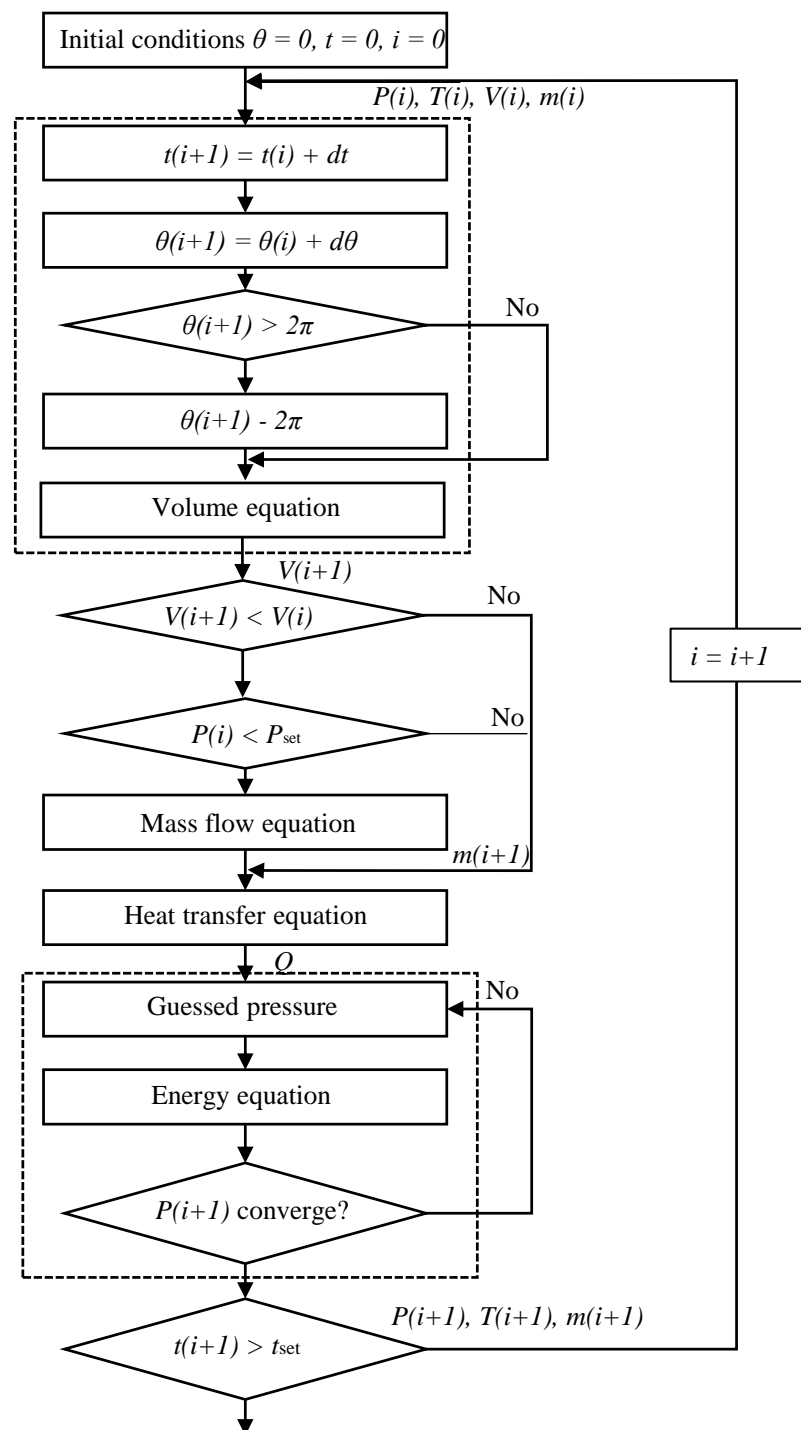


Figure 6. The flowchart for the model algorithm.

4. Experimental Apparatus

The experimental apparatus consisted of a diaphragm compressor which is described in Section 2, the experiment process is a simple open layout. According to Figure 7, the intake air passes through a flow meter and gets into the compressor, in the compressor the pressure is increased and after temperature and pressure measurements, the air exits to the ambient through the throttle valve.

The system has the advantage of using a dual scale RS pro gauge pressure sensor with a maximum measurement of 10 bar, its ambient operating temperature of it is in the range of -40 to $+60$ °C with the accuracy of $\pm 25\%$ of the pressure reading. These

kinds of gauges are designed based on the bourdon tube principle and can be used for small-scale compressors or HVAC systems and able to work with liquid and gas. In the experiment, Platon flow meter with the maximum operating pressure of 7 bar is used. The maximum operating temperature is 55 °C and can measure up to 100 lit/min of flow rate. The accuracy of the flow meter is 5 lit/min.

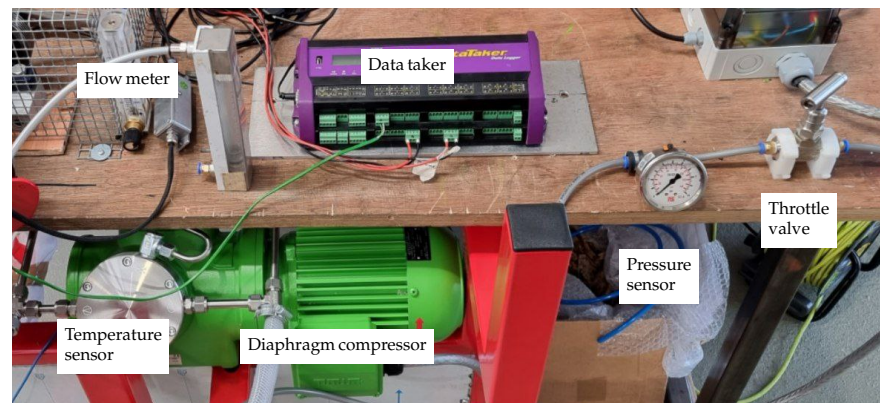
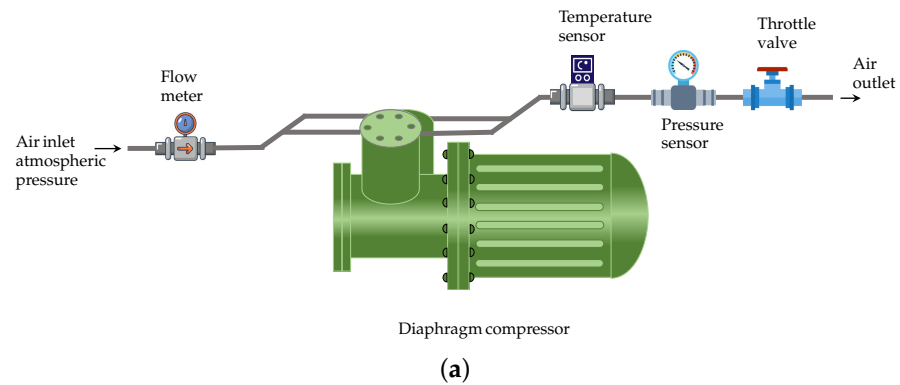


Figure 7. Experimental apparatus (a) schematic, and (b) the laboratory apparatus of the experimental model. The system has flow, temperature, and pressure sensors and the compression ratio is adjustable in the system.

Because of the lack of high pressure or vacuum tank, the lab test was restricted to compression operation. Therefore, the data from compressor supplier datasheet is used to validate the model and simulation between 0.2 and 1 bar (the vacuum pump operation) (https://knf.com/fileadmin/Global_files/Downloads/Product_OEM_Process/Datasheets/Datasheet_N_186-1-2_01-2019_web.pdf (accessed on 1 January 2019)). The comparison of the calculated air flow rates and the experimental data provided by the compressor supplier is shown in Figure 8. For compression operation (pressure between 1 and 6 bar) the experimental apparatus in Figure 7b is used (apart from the manufacturer datasheet). The rotational speed is constant (640 rpm) and the pressure difference for opening the reed valve is set at 0.01 bar. The inlet flow rate needs to be measured, therefore, the flow meter is installed at the diaphragm compressor inlet. The outlet is connected to a pressure-measuring gauge and a throttle valve. The outlet pressure is changed by the throttle valve and the pressure is adjusted by observing the pressure measurement gauge, the aim is to measure the inlet flow meter value. At the same time, the outlet temperature is measured using a data acquisition unit and a k-type thermocouple. The compressor power is measured using power meters. The temperature is monitored once the outlet pressure is changed with a waiting time for the temperature stabilisation before reading it. The rotational speed of 640 rpm is used for the compressor in the operation cycle and remains constant in any conditions.

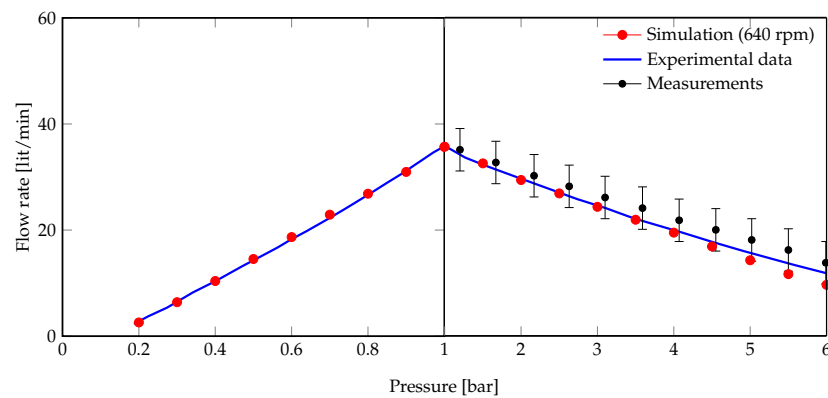


Figure 8. The flow rate profile against pressure; the red circle indicates the simulation results for the speed of 640 rpm, the blue line indicates the manufacturer data, and the black circle indicates the results from the experimental data that performed in Figure 7.

5. Results and Discussion

In order to understand if the model is working properly, in the first step the model needs to be validated, therefore further analysis are carried on to analyse the compressor efficiency and the sensitivity analysis of the effective parameters on the performance of the compressor.

5.1. Model Validation

As shown in Figure 8, the simulation results agree quite well with the experimental results when the ambient air is compressed to no more than 2 bar (abs). The prediction errors are getting larger when the back pressure of the compressor is higher. The detailed modelling of the reed valve is required to further improve the accuracy of the simulation. There is some overshooting difference between the experimental results and the modelling simulation which are due to the experimental instruments uncertainties which are defined as the instrument accuracy.

the diaphragm motion was set to vertical up and down in order to simplify the modelling process, in reality the diaphragm motion is more complex, the piston twists and the diaphragm deforms elastically, so more accurate modelling requires the use of 3D software and consideration of the diaphragm material.

5.2. Flow Rate

From the experimental results (Table 3), the inlet temperature is almost constant (33 ± 1 °C). The ambient pressure is 1 bar; according to Table 3, increasing the pressure from 0 to 6 bar (gauge) results in the flow rate reduction (from 38 to 14 lit/min) for flow compression. Increasing the pressure from -0.2 to 0 bar (gauge) advances the flow rate (from 2 to 38 lit/min) for vacuum operation.

Table 3. The experimental results.

Pressure [bar]	0	0.5	1	1.5	2	2.5	3	3.5	4	4.5	5	5.5	6
Flow rate [Lit/min]	42	38	35	32.5	30	29	26	25	22.5	20	19	16	14
Temperature [°C]	32.5	32.9	33	33.1	33.4	33.6	33.7	33.8	33.7	32.6	32.4	32.2	32.2

As it is stated, an increase in pressure leads to a flow rate decrease. It is possible, however, the flow rate changes due to ambient or inlet temperatures. Figure 9a shows that the lower ambient temperature (T_{amb}) lead to a lower flow rate; dropping the ambient temperature from 40 to 5 °C can lead to a 7 lit/min drop in the flow rate once the pressure is 1 bar. However, the effect of ambient temperature on the flow rate tends to reduce at

higher pressures (6 bar), where a decrease in ambient temperature from 40 to 5 °C only reduces the flow rate by 1 lit/min drop.

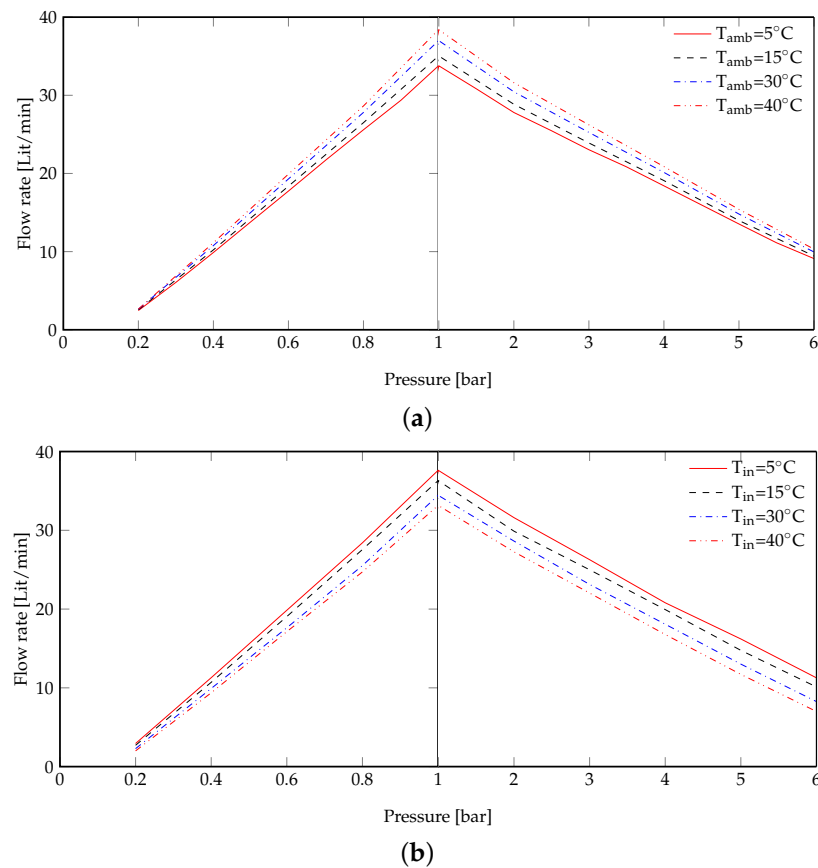


Figure 9. The effect of (a) ambient temperature and, (b) gas inlet temperature on the diaphragm compressor flow rate for pressure range between 1 and 6 bar (gauge).

There is a possibility that the temperature difference between the gas and the ambient has been increased at higher pressures. It is due to the fact that the gas temperature increases in the chamber. Although heat loss between chambers and ambient exists, the heat transfer between compressor and ambient is poor due to the small time span in each cycle; therefore, the effect of ambient temperature on flow rate at high pressures (over 4 bar) is not considerable. However, most of the input values in the model come from the manufacturer's data sheet or physical observation of the compressor in the lab. Therefore, there might other parameters inside the compressor which are not considered and may result in deviations in the graph.

A second parameter that can affect system performance is the inlet gas temperature (T_{in}), which has a reductive effect on the flow rate. Increasing the inlet gas temperature from 5 to 40 degrees Celsius can reduce the flow rate by a 7 lit/min drop, and this reduction is almost constant at all pressure levels in the compression process. However, for vacuum operations, the reductive effect of increasing the ambient temperature is falling from a 7 lit/min drop at 1 bar to a zero drop effect at 0.2 bar.

In Figure 10, it is indicated that the compressor has two chambers that work in a 90-degree phase difference. In the intake stage, flow rate profiles peak smaller (0.001 lit/min), but with a longer time frame (0.03 s). On the other hand, the flow rate profile peaks are almost 2.5 times higher than the intake flow rate peaks (Figure 10b), but they are sharper which shows that the exhaust process has a shorter time of action (0.015 s) and it is half of than intake process. Nevertheless, the area under the intake and exhaust profiles, which represents the mass of gas inside the chamber, is equal according to the laws of conservation of mass or continuity.

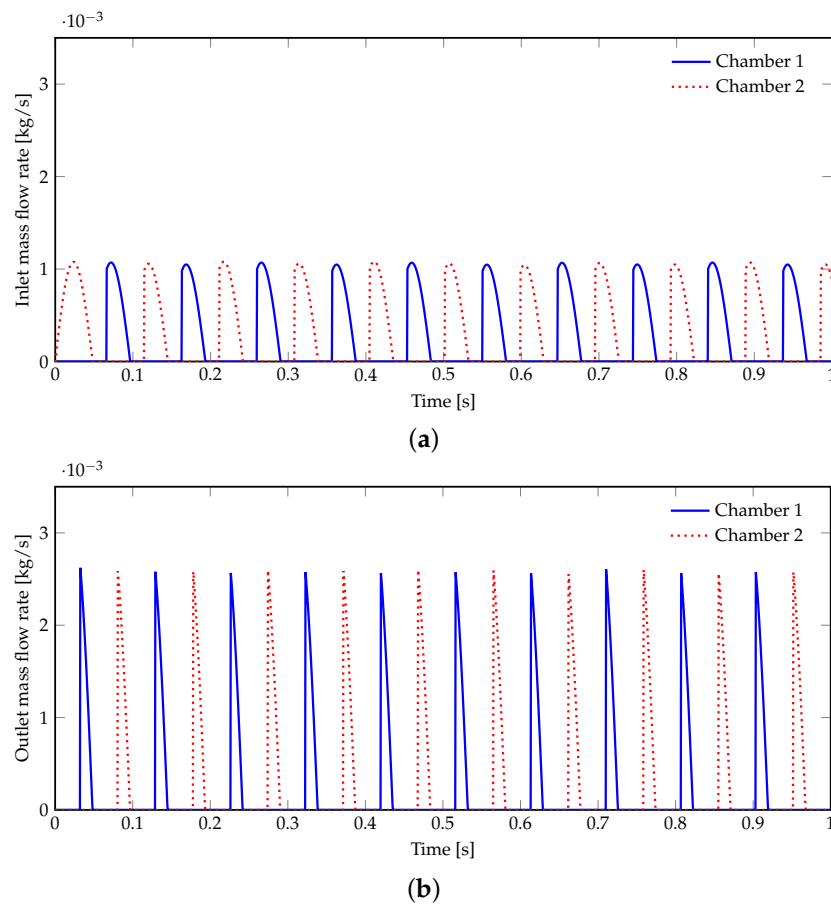


Figure 10. The mass flow rate of the compressor for (a) inlet gas, and (b) outlet gas, for both chambers (the chambers work in 90° phase difference).

5.3. Pressure Ratio

The pressure ratio (R_c) is defined as the ratio of the outlet pressure to the inlet pressure of the diaphragm compressor. For constant inlet pressure (1 bar) to the compressor, the pressure-volume diagram for compression ratios from 2 to 6 is shown in Figure 11. The chamber volume is 0.033 lit, the higher the compression ratio leads to the larger output pressure and as a result lower chamber internal volume change during the isobaric processes of the compression cycle. Lower volume change in the isobaric process means the exhaust reed valve is opened and the crankshaft is at the highest possible height.

Furthermore, an increase in the compression ratio tends to increase the outlet gas temperature of the chambers. Once the compression ratio is increased from 2 to 5, it is predicted that the outlet temperature will climb from 42 to 57 °C. Additionally, higher compression ratios result in wider compression-discharges and shorter expansion-intakes.

Figure 12a,b illustrates the variations of the working gas temperatures and pressures inside the compressor over operating time. As can be seen, both the temperature and pressure increase during the compression of the gas and reach their peaks. During discharging, the compressor gas temperature and pressure are reduced to the minimum level close to ambient conditions. It should be noted that due to the pressure drop during the expansion at the empty chamber (in this stage the hot gas is discharged) a low-pressure regime—which is almost vacuum—is created in the chamber, once the inlet gas enters the chamber from the inlet valve due to the pressure drop their temperature drops even lower than the inlet temperature. This drop can be seen as intensified with the increase in compression ratios. Moreover, the rate of the temperature rise between compression ratio can be observed to be decreasing. For instance, the temperature difference between the compression ratio of 2 and 3 is 6.5 °C, while the change between the compression ratio of 3 and 4 is 5.1 °C. This

can be due to the fact that gas with a higher temperature leading to higher compressor heat losses, so at a higher pressure, the increased rate of temperature gradually drops.

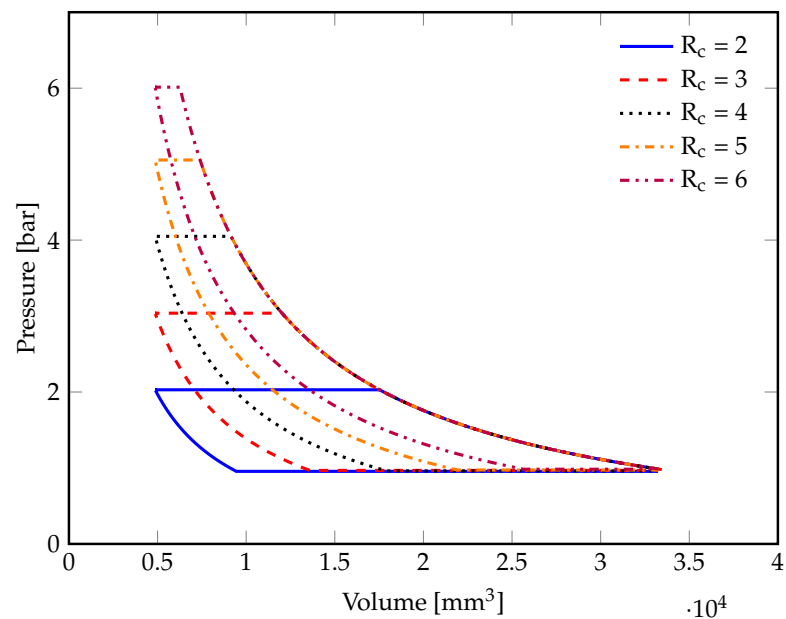
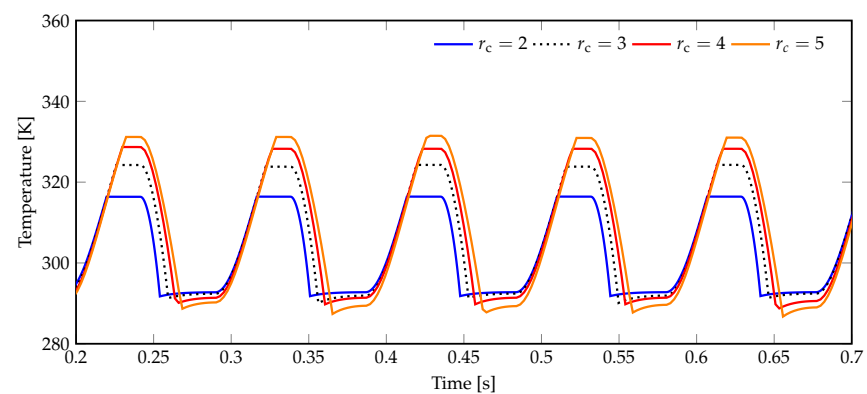
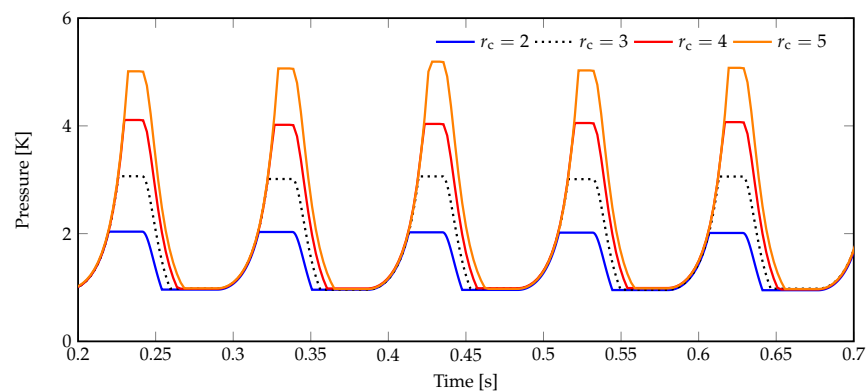


Figure 11. The pressure-volume diagram of the compressor for a range of pressure ratio ($2 \leq R_c \leq 6$) with 1 unit increment.



(a)



(b)

Figure 12. The simulation results for cyclic behaviour of the compressor in (a) gas temperature and (b) gas pressure, inside the compressor chamber.

6. Conclusions

Characterisation and optimisation of compressors always depend on the accuracy of the model used. Our objective is to investigate the modelling of oscillating diaphragm compressors (which have the advantage of using an oscillating diaphragm driven by a crank mechanism) using MATLAB simulations. An average efficiency of 70% is achieved with a compressor that runs at a constant power of 200 W. The performance of the compressor is evaluated by the reciprocating motion of the diaphragm. By considering the diaphragm compressor's geometrical characteristics, a model is developed for analysing its kinematics. By evaluating the energy balance through the thermodynamic cycle, equations can be used to determine the thermodynamic state of the compressor. With the properties of real gas assumptions, the air is assumed to be the operating fluid. To evaluate the validity of the model, an experimental setup is performed. Another validation of the model is also performed based on the manufacturer datasheet once the vacuum pump mode is used for 0.2 to 1 bar. The model is understood to be in reasonable agreement with both experimental design and manufacturer experiments. Flow rate is examined as a function of ambient temperature, gas inlet temperature, and chamber pressure, and it is shown that compressor operation with lower ambient air can result in a slight decrease in mass flow rate. On the other hand, decreasing the inlet temperature can result in an improvement in the outlet mass flow rate. Likewise, the model response to compression ratio is studied, and the compressor's work is calculated in the range of 1 to 6 bar, which allows the value provided by the manufacturer to be validated. The compression ratio is also investigated in relation to all stages of the compressor cycle (compression, expansion, suction, and discharge) and an increase in the compression ratio tends to increase the outlet gas temperature of the chambers.

Author Contributions: Conceptualisation, S.M., A.N. and Z.M.; Methodology, A.N., S.M. and H.B.; Modelling, S.M. and Z.M.; Validation, A.N.; Investigation, A.N.; Writing—original draft, A.N., S.M. and Z.M.; Supervision, Z.M., H.B. and T.R. All authors have read and agreed to the published version of the manuscript.

Funding: The authors gratefully acknowledge the support from the Solar S&HP project, coded (EP/T023090/1), and funded by the Engineering and Physical Science Research Council (EPSRC) of the UK.

Data Availability Statement: Data available on request due to restrictions eg privacy or ethical The data presented in this study are available on request from the corresponding author.

Conflicts of Interest: The authors declare no conflict of interests.

References

1. Lyu, L.; Chen, W.; Kan, A.; Zhang, Y.; Xue, S.; Zeng, J. Investigation of a Dual-Loop ORC for the Waste Heat Recovery of a Marine Main Engine. *Energies* **2022**, *15*, 8365. [[CrossRef](#)]
2. Counsell, J.; Khalid, Y.; Stewart, M. Comparative performance modelling of heat pump based heating systems using dynamic carbon intensity. In Proceedings of the 11th IET International Conference on Advances in Power System Control, Operation and Management (APSCOM 2018), Hong Kong, China, 11–15 November 2018.
3. Meibodi, S.S.; Loveridge, F. The future role of energy geostructures in fifth generation district heating and cooling networks. *Energy* **2022**, *240*, 122481. [[CrossRef](#)]
4. Ocvirk, M.; Ristić, A.; Zabukovec Logar, N. Synthesis of Mesoporous γ -Alumina Support for Water Composite Sorbents for Low Temperature Sorption Heat Storage. *Energies* **2021**, *14*, 7809. [[CrossRef](#)]
5. Bao, H.; Ma, Z.; Roskilly, A.P. A chemisorption power generation cycle with multi-stage expansion driven by low grade heat. *Energy Convers. Manag.* **2017**, *150*, 956–965. [[CrossRef](#)]
6. Von Platen, B.C.; Munters, C.G. Refrigerator. US patent US1685764A, 1 October 1925.
7. Najjaran, A.; Freeman, J.; Ramos, A.; Markides, C.N. Experimental investigation of an ammonia-water-hydrogen diffusion absorption refrigerator. *Appl. Energy* **2019**, *256*, 113899. [[CrossRef](#)]
8. Najjaran, A.; Harraz, A.A.; Mac Dowell, N.; Markides, C. Numerical and experimental investigation of diffusion absorption refrigeration systems for use with low-temperature heat sources. In Proceedings of the Ecos 2018—The 31st International Conference on Efficiency, Cost, Optimization, Simulation Furthermore, Environmental Impact Of Energy Systems, Guimaraes, Portugal, 17–22 June 2018; pp. 17–22.

9. Rattner, A.S.; Garimella, S. Low-source-temperature diffusion absorption refrigeration. part II: experiments and model assessment. *Int. J. Refrig.* **2016**, *65*, 312–329. [[CrossRef](#)]
10. Rattner, A.S.; Garimella, S. Coupling-fluid heated bubble pump generators: Experiments and model development. *Sci. Technol. Built Environ.* **2015**, *21*, 332–347. [[CrossRef](#)]
11. Ma, Z.; Bao, H.; Roskilly, A.P. Electricity-assisted thermochemical sorption system for seasonal solar energy storage. *Energy Convers. Manag.* **2020**, *209*, 112659. [[CrossRef](#)]
12. Thinsurat, K.; Ma, Z.; Roskilly, A.P.; Bao, H. Compressor-assisted thermochemical sorption integrated with solar photovoltaic-thermal collector for seasonal solar thermal energy storage. *Energy Convers. Manag. X* **2022**, *15*, 100248. [[CrossRef](#)]
13. Fitó, J.; Coronas, A.; Mauran, S.; Mazet, N.; Perier-Muzet, M.; Stitou, D. Hybrid system combining mechanical compression and thermochemical storage of ammonia vapor for cold production. *Energy Convers. Manag.* **2019**, *180*, 709–723. [[CrossRef](#)]
14. Gao, P.; Hu, H.; Jin, S.; Wang, S.; Chen, Y.; Wu, W.; Yang, Q.; Zhu, F.; Wang, L. Solar-driven compression-assisted desorption chemisorption refrigeration/cold energy storage system. *Energy Convers. Manag.* **2022**, *258*, 115474. [[CrossRef](#)]
15. Steger, D.; Feist, M.; Schlücker, E. Using a screw-type machine as reversible compressor–expander in a Carnot Battery: An analytical study towards efficiency. *Appl. Energy* **2022**, *316*, 118950. [[CrossRef](#)]
16. Oh, S.; Wang, S.; Cho, S. Development of Energy Efficiency Design Map based on acoustic resonance frequency of suction muffler in compressor. *Appl. Energy* **2015**, *150*, 233–244. [[CrossRef](#)]
17. Bianchi, G.; Cipollone, R. Theoretical modeling and experimental investigations for the improvement of the mechanical efficiency in sliding vane rotary compressors. *Appl. Energy* **2015**, *142*, 95–107. [[CrossRef](#)]
18. Zhao, Y.; Xu, X.; Qadrdan, M.; Wu, J. Optimal operation of compressor units in gas networks to provide flexibility to power systems. *Appl. Energy* **2021**, *290*, 116740. [[CrossRef](#)]
19. Meroni, A.; Zühlsdorf, B.; Elmegaard, B.; Haglind, F. Design of centrifugal compressors for heat pump systems. *Appl. Energy* **2018**, *232*, 139–156. [[CrossRef](#)]
20. Uusitalo, A.; Turunen-Saaresti, T.; Honkatukia, J.; Tiainen, J.; Jaatinen-Värri, A. Numerical analysis of working fluids for large scale centrifugal compressor driven cascade heat pumps upgrading waste heat. *Appl. Energy* **2020**, *269*, 115056. [[CrossRef](#)]
21. Tirnovan, R.; Giurgea, S.; Miraoui, A.; Cirrincione, M. Surrogate modelling of compressor characteristics for fuel-cell applications. *Appl. Energy* **2008**, *85*, 394–403. [[CrossRef](#)]
22. Viholainen, J.; Grönman, K.; Jaatinen-Värri, A.; Grönman, A.; Ukkonen, P.; Luoranen, M. Centrifugal compressor efficiency improvement and its environmental impact in waste water treatment. *Energy Convers. Manag.* **2015**, *101*, 336–342. [[CrossRef](#)]
23. Olsson, A.; Stemme, G.; Stemme, E. A numerical design study of the valveless diffuser pump using a lumped-mass model. *J. Micromech. Microeng.* **1999**, *9*, 34. [[CrossRef](#)]
24. Venkatesan, J.; Nagarajan, G.; Seeniraj, R.; Murugan, R. Experimental validation of a mathematical model of a reed-valve reciprocating air compressor from an automotive-braking system. *Int. J. Automot. Technol.* **2010**, *11*, 317–322. [[CrossRef](#)]
25. Sathe, A.A.; Groll, E.A.; Garimella, S.V. Analytical model for an electrostatically actuated miniature diaphragm compressor. *J. Micromech. Microeng.* **2008**, *18*, 035010. [[CrossRef](#)]
26. Guan, D.; Cong, X.; Li, J.; Niu, Z. Experimental test and theoretical modeling on the working characteristics of spherical water pump. *Flow Meas. Instrum.* **2022**, *85*, 102162. [[CrossRef](#)]
27. Adair, R.P.; Qvale, E.B.; Pearson, J.T. Instantaneous heat transfer to the cylinder wall in reciprocating compressors. In Proceedings of the International Compressor Engineering Conference, West Lafayette, IN, USA, 17–20 July 1972.
28. Jia, X.; Zhao, Y.; Chen, J.; Peng, X. Research on the flowrate and diaphragm movement in a diaphragm compressor for a hydrogen refueling station. *Int. J. Hydrog. Energy* **2016**, *41*, 14842–14851. [[CrossRef](#)]
29. Tuhovcak, J.; Hejčík, J.; Jícha, M. Modelling fluid flow in a reciprocating compressor. *Epj Web Conf.* **2015**, *92*, 02100. [[CrossRef](#)]
30. Picard, A.; Davis, R.; Gläser, M.; Fujii, K. Revised formula for the density of moist air (CIPM-2007). *Metrologia* **2008**, *45*, 149. [[CrossRef](#)]
31. Lemmon, E.W.; Jacobsen, R.T.; Penoncello, S.G.; Friend, D.G. Thermodynamic properties of air and mixtures of nitrogen, argon, and oxygen from 60 to 2000 K at pressures to 2000 MPa. *J. Phys. Chem. Ref. Data* **2000**, *29*, 331–385. [[CrossRef](#)]

Disclaimer/Publisher’s Note: The statements, opinions and data contained in all publications are solely those of the individual author(s) and contributor(s) and not of MDPI and/or the editor(s). MDPI and/or the editor(s) disclaim responsibility for any injury to people or property resulting from any ideas, methods, instructions or products referred to in the content.